

## PROBING INHOMOGENEOUS BLAZAR HEATING WITH THE LY $\alpha$ FOREST

ASTRID LAMBERTS<sup>1</sup>, EWALD PUCHWEIN<sup>2</sup>, PHILIP CHANG<sup>3</sup>, CHRISTOPH PFROMMER<sup>4</sup>, AVERY E. BRODERICK<sup>5,6</sup> AND MOHAMAD SHALABY<sup>5,6</sup>

<sup>1</sup> Theoretical Astrophysics, California Institute of Technology, Pasadena, CA, 91125, USA

<sup>2</sup> Institute of Astronomy and Kavli Institute for Cosmology, University of Cambridge, Madingley Road, Cambridge, CB3 0HA, UK

<sup>3</sup> Department of Physics, University of Wisconsin-Milwaukee, 1900 East Kenwood Boulevard, Milwaukee WI 53211, USA

<sup>4</sup> Heidelberg Institute for Theoretical Studies, Schloss-Wolfsbrunnenweg 35, D-69118 Heidelberg, Germany

<sup>5</sup> Perimeter Institute for Theoretical Physics, 31 Caroline Street North, Waterloo, ON, N2L 2Y5, Canada and

<sup>6</sup> Department of Physics and Astronomy, University of Waterloo, 200 University Avenue West, Waterloo, ON, N2L 3G1, Canada

*Draft version February 12, 2017*

### ABSTRACT

#### 1. INTRODUCTION

Only 10% of the baryons in the present-day universe are in collapsed structures such as galaxies, clusters and groups (Shull et al. 2012). The vast majority of ordinary matter is in a more diffuse state around galaxies (forming the circumgalactic medium) and between them, forming the intergalactic medium (IGM, see McQuinn 2016, for a recent review). The latter is composed of gas around and below the cosmic mean density  $\Delta$ . As such, its evolution is mostly linear, closely follows the underlying dark matter and is directly influenced by fundamental cosmological parameters (Palanque-Delabrouille et al. 2013; Slosar et al. 2013; Palanque-Delabrouille et al. 2015). As the main reservoir for baryons, its physical state sets the initial conditions for star formation.

Because of its linear nature, the IGM is an excellent calorimeter of energy injected by star formation and active galactic nuclei (AGN). More specifically, re-ionization of H and HeI around  $z \simeq 10 - 6$  (Fan et al. 2006) and then HeII around  $z \geq 3.5$  provide most of the heat input in the IGM (McQuinn et al. 2009; Worseck et al. 2011). Subsequently, the evolution of the IGM is set by the balance between photoheating and adiabatic cooling. As a result the IGM globally cools, with the lowest density gas cooling faster, yielding a tight temperature-density relation  $T = T_0 \Delta^{\gamma-1}$  where  $T_0$  is the temperature at the mean density and  $\gamma \simeq 1.6$  for low density gas (Hui & Gnedin 1997). Recent models of HeII re-ionisation, based on cosmological simulations including complete radiative transfer, indicate a patchy process yielding a broadening of the temperature-density distribution around mean density for  $z \simeq 3$  (Meiksin & Tittley 2012; Compostella et al. 2013).

The most dramatic impact on the low-density IGM could come from TeV-blazar heating (Chang et al. 2012; Puchwein et al. 2012; Lamberts et al. 2015), with potential impact on structure formation (Pfrommer et al. 2012). This model is based on the electron/positron beams that result from the annihilation of very high energy gamma-rays from blazars on the extragalactic background light. They can be subject to plasma instabilities, which efficiently redistribute their kinetic energy to the surrounding intergalactic medium (Broderick et al. 2012; Schlickeiser et al. 2013, 2012; Chang et al. 2014, 2016), but see Miniati & Elyiv (2013); Sironi & Giannios (2014).

[Need paragraph about fermi stuff and quasar and blazar evolution here]

The resulting heating is only limited by the number of TeV-photons, which makes it a competitive heating source in the underdense regions, where photoheating is rendered impossible as the recombination time is larger than the Hubble time. Assuming a uniform heating rate, it results in an inverted temperature-density distribution below the cosmic mean, with low density gas reaching  $10^5$ K at  $z = 3$  and  $\simeq 10^6$ K in the present-day universe (Puchwein et al. 2012).

While uniform heating is a reasonable first order approximation, in Lamberts et al. (2015, hereafter Paper I) we showed that it is affected by the clustering of blazars. As a result, regions close to large overdense regions such as clusters or groups are receiving more heat than remote regions mostly surrounded by voids. In our favoured model, where TeV blazars have the same bias than quasars, there are almost two orders of magnitude between the hottest and warmest gas between  $z \simeq 2 - 3$  although the bulk of the gas follows a temperature consistent with the uniform model. By the present day, all regions have been heated up and the uniform model provides a good description of the impact of blazar heating.

Observational confirmation of blazar heating is a challenge, because it mostly affects low-density regions. The IGM is mostly observed through absorption lines within the spectra of distant quasars, due to a tiny fraction of neutral hydrogen (Lynds 1971). The so-called Ly $\alpha$  forest can be observed with ground-based facilities for  $z \geq 1.7$  and a variety of statistics have been developed to analyse spectra from a wide range of instruments. However, deriving the physical parameters of the IGM from the different statistics requires a careful comparison with cosmological simulations (see e.g. Rauch et al. 1997; Schaye et al. 2000; Becker & Bolton 2013; Bolton et al. 2017). Because of the intrinsic observational challenges, numerical shortcomings and difficulty to establish the validity of the different statistics, there is no observational consensus on the thermal state of the low-density IGM.

Based on the probability distribution function (PDF) of the transmitted flux, Kim et al. (2007); Bolton et al. (2008); Viel et al. (2009); Calura et al. (2012) find that an isothermal ( $\gamma = 1$ ) or inverted ( $\gamma \leq 1$ ) are in good agreement with the data. However, the flux PDF can be strongly affected by systematic errors in the continuum placement (Lee 2012) and sample variance (Rollinde

et al. 2013). Analysis of the curvature of the Ly $\alpha$  spectrum (Becker et al. 2011; Boera et al. 2014) prefers a warmer temperature of the IGM. However, this method, which is based on the smoothness of the spectrum, is mostly sensitive to densities above the mean, especially at low redshift. Finally, Voight profile fitting of the spectra yields the distribution of line-width (b) versus HI column density ( $N_{HI}$ ). Using the lower envelope of the distribution as a proxy for the  $T - \rho$  relation, Rudie et al. (2012); Bolton et al. (2014) find no evidence of blazar heating.

Based a unique spectrum, with exceptional signal-to-noise (S/N) and resolution, Rorai et al. (2017) can rescale the optical depth to enhance the signal from low-density regions. At the considered redshifts ( $2.5 \leq z \leq 3$ ), they do find that the high end of the transmitted flux probability distribution is better matched by a broken power-law for the temperature-density distribution, with an inverted slope at the low density end. Their model including temperature fluctuations at low densities produces a satisfactory match as well. The authors also perform a careful analysis of the power spectrum and lower envelope of the “ $b - N_{HI}$ ” distribution and show they are largely unsensitive to the low-density regions.

### [Do we need a paragraph about low-z measurements?]

In this paper, we perform confront our model for inhomogeneous blazar heating with observational data. We first describe the numerical simulations we use to model the IGM (§2) and the resulting observables we derive (§3). We then discuss the direct comparison with observations (§4) and conclude (§5).

## 2. COSMOLOGICAL SIMULATIONS

Our simulations are very similar to the simulations presented in Paper I and are performed at higher resolution. In this section we remind the reader of their relevant characteristics.

We perform our simulations with GADGET-3, which is and upgraded version of GADGET-2 (Springel 2005). It is based on a Smoothed Particle Hydrodynamics (SPH) scheme and solves the gravitational evolution of gas and dark matter with a TREE-PM N-body method. The equations of hydrodynamics are solved with an entropy conserving scheme based on (Springel & Hernquist 2002). Our simulations are based on the cosmological parameters based on the *Planck* data combined with lensing, *WMAP* and high multipole measurements (Planck Collaboration et al. 2014):  $\Omega_M = 0.305$ ,  $\Omega_\lambda = 0.694$ ,  $\Omega_B = 0.0481$ ,  $h = 0.679$ ,  $\sigma_8 = 0.827$  and  $n_s = 0.962$ . These values are slightly updated with respect to the simulations presented in (Puchwein et al. 2012; Lamberts et al. 2015). [I don't expect this to have any influence, is that correct?]

We start our simulations based on initial conditions evolved up to redshift  $z = 110$  and stop our simulations at  $z = 1.74$ , beyond which observational date is sparse and underdense regions not well sampled. As this work focusses on the IGM, we use a simplified model for star formation, where gas particles with density  $\delta_{\text{gas}} \geq 1000$  and  $T \leq 10^5$  are directly converted into stars (Viel et al. 2004). While this can yield inaccurate galaxy properties, it does not affect the low-density IGM and significantly speeds up the simulations. We also neglect direct black

hole feedback.

### [Paragraph about UV background and related stuff here]

We perform a set of three simulations, one without any blazar heating, one with uniform blazar heating and one with inhomogeneous blazar heating. The uniform blazar heating model is identical to the “intermediate heating” model presented in Puchwein et al. (2012). Our inhomogeneous model has the same total amount of energy injected by blazars while accounting for regions receiving more or less heating according to their proximity to heating sources. The model is fully described in Paper I and is based on an analytic formalism relating the distribution of the heating rate to the underlying dark matter distribution. It results in the filtering function shown on Fig. 1, which removes small scale fluctuations and enhances fluctuations beyond  $\simeq 10 h^{-1} \text{ Mpc}$  at  $z = 4$  and  $\simeq 40 h^{-1} \text{ Mpc}$  at  $z = 2$ . The shape and redshift evolution of the window function is set by the mean free path of the VHEGR combined with the bias of the heating sources. While we presented two models in Paper I, with galaxy bias and quasar bias, in this work we focus on the model with quasar bias, which is probably more representative of the bias of TeV blazars.

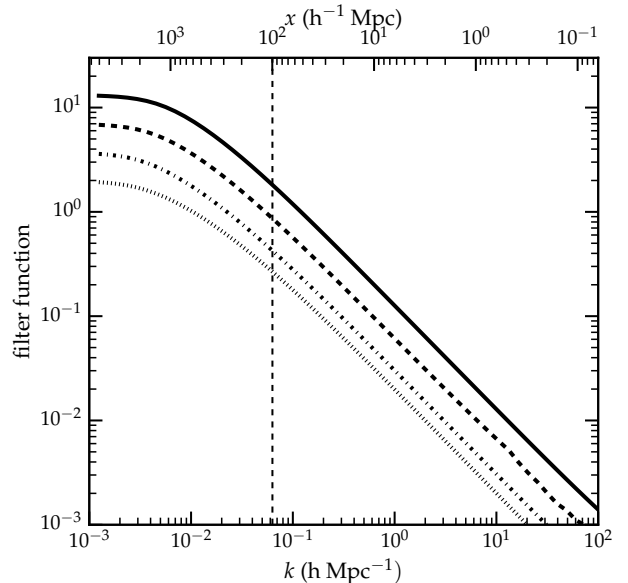


FIG. 1.— Window function for TeV blazar heating for  $z = 1$  (dotted line),  $z = 2$  (dot-dashed line),  $z = 3$  (dashed line) and  $z = 4$  (solid line). The vertical dashed line indicate the minimal comoving wavenumber modeled in the simulation.

Because of the typical length scale of the heating rate fluctuations, our simulation have a comoving sidelength of a  $100 h^{-1} \text{ Mpc}$ . Tests in Paper I showed that this is a sufficiently large size to properly sample the full range of temperature fluctuations. **Discuss resolution here**

## 3. COMPARISON WITH OBSERVATIONS

### 3.1. Inhomogenous blazar heating

Fig. 2 shows the temperature-density distribution in our inhomogeneous heating model. The complete description of the inhomogeneous heating model are described in Paper I. Here we recall the main characteristics

of the temperature-density distribution, which most observations try to infer. As time goes by, the cumulated impact of blazar heating increases, with a higher temperature difference with respect to the unheated case. Still, as some regions are too far from heating sources, they remain cold, as can be seen by the remnant cold gas, especially at  $z = 3$ . This is very different from the uniform heating model (shown in black) and can potentially reconcile the blazar heating model with observations of absorption lines with Doppler parameter ( $b \leq 20 \text{ km s}^{-1}$ ). At the redshifts most accessible with the Ly $\alpha$  forest, the temperature range covers almost two orders of magnitude at the lowest density and even around mean density, there is an important spread. At lower redshifts, the whole IGM gets heated up and after  $z \geq 1$ , the inhomogeneous model recovers the uniform model. In the following section, we compare the observables derived from this  $T - \rho$  distribution with observational data.

### 3.2. Post-processing the simulations

- Global flow , potential caveats
- Details about subdividing LOS in chunks for VP-FIT

### 3.3. Ly $\alpha$ forest statistics

#### 3.4. Thermal state of the IGM

1. Compare with Rorai 2016
2. Maybe compare with low-z results
3. Rudie and other b-Nh distributions

## 4. DISCUSSION

## 5. CONCLUSIONS

## REFERENCES

- Becker, G. D., & Bolton, J. S. 2013, MNRAS, 436, 1023  
 Becker, G. D., Bolton, J. S., Haehnelt, M. G., & Sargent, W. L. W. 2011, MNRAS, 410, 1096  
 Boera, E., Murphy, M. T., Becker, G. D., & Bolton, J. S. 2014, MNRAS, 441, 1916  
 Bolton, J. S., Becker, G. D., Haehnelt, M. G., & Viel, M. 2014, MNRAS, 438, 2499  
 Bolton, J. S., Puchwein, E., Sijacki, D., et al. 2017, MNRAS, 464, 897  
 Bolton, J. S., Viel, M., Kim, T.-S., Haehnelt, M. G., & Carswell, R. F. 2008, MNRAS, 386, 1131  
 Broderick, A. E., Chang, P., & Pfrommer, C. 2012, ApJ, 752, 22  
 Calura, F., Tescari, E., D'Odorico, V., et al. 2012, MNRAS, 422, 3019  
 Chang, P., Broderick, A. E., & Pfrommer, C. 2012, ApJ, 752, 23  
 Chang, P., Broderick, A. E., Pfrommer, C., et al. 2014, ApJ, 797, 110  
 —. 2016, ApJ, 833, 118  
 Compostella, M., Cantalupo, S., & Porciani, C. 2013, MNRAS, 435, 3169  
 Fan, X., Carilli, C. L., & Keating, B. 2006, ARA&A, 44, 415  
 Hui, L., & Gnedin, N. Y. 1997, MNRAS, 292, 27  
 Kim, T.-S., Bolton, J. S., Viel, M., Haehnelt, M. G., & Carswell, R. F. 2007, MNRAS, 382, 1657  
 Lamberts, A., Chang, P., Pfrommer, C., et al. 2015, ApJ, 811, 19  
 Lee, K.-G. 2012, ApJ, 753, 136  
 Lynds, R. 1971, ApJ, 164, L73  
 McQuinn, M. 2016, ARA&A, 54, 313  
 McQuinn, M., Lidz, A., Zaldarriaga, M., et al. 2009, ApJ, 694, 842  
 Meiksin, A., & Tittley, E. R. 2012, MNRAS, 423, 7  
 Miniati, F., & Elyiv, A. 2013, ApJ, 770, 54  
 Palanque-Delabrouille, N., Yèche, C., Borde, A., et al. 2013, A&A, 559, A85  
 Palanque-Delabrouille, N., Yèche, C., Baur, J., et al. 2015, JCAP, 11, 011  
 Pfrommer, C., Chang, P., & Broderick, A. E. 2012, ApJ, 752, 24  
 Planck Collaboration, Ade, P. A. R., Aghanim, N., et al. 2014, A&A, 571, A16  
 Puchwein, E., Pfrommer, C., Springel, V., Broderick, A. E., & Chang, P. 2012, MNRAS, 423, 149  
 Rauch, M., Miralda-Escude, J., Sargent, W. L. W., et al. 1997, ApJ, 489, 7  
 Rollinde, E., Theuns, T., Schaye, J., Pâris, I., & Petitjean, P. 2013, MNRAS, 428, 540  
 Rorai, A., Becker, G. D., Haehnelt, M. G., et al. 2017, MNRAS, 466, 2690  
 Rudie, G. C., Steidel, C. C., & Pettini, M. 2012, ApJ, 757, L30  
 Schaye, J., Theuns, T., Rauch, M., Efstathiou, G., & Sargent, W. L. W. 2000, MNRAS, 318, 817  
 Schlickeiser, R., Ibscher, D., & Supsar, M. 2012, ApJ, 758, 102  
 Schlickeiser, R., Krakau, S., & Supsar, M. 2013, ApJ, 777, 49  
 Shull, J. M., Smith, B. D., & Danforth, C. W. 2012, ApJ, 759, 23  
 Sironi, L., & Giannios, D. 2014, ApJ, 787, 49  
 Slosar, A., Iršič, V., Kirkby, D., et al. 2013, JCAP, 4, 026  
 Springel, V. 2005, MNRAS, 364, 1105  
 Springel, V., & Hernquist, L. 2002, MNRAS, 333, 649  
 Viel, M., Bolton, J. S., & Haehnelt, M. G. 2009, MNRAS, 399, L39  
 Viel, M., Haehnelt, M. G., & Springel, V. 2004, MNRAS, 354, 684  
 Worseck, G., Prochaska, J. X., McQuinn, M., et al. 2011, ApJ, 733, L24

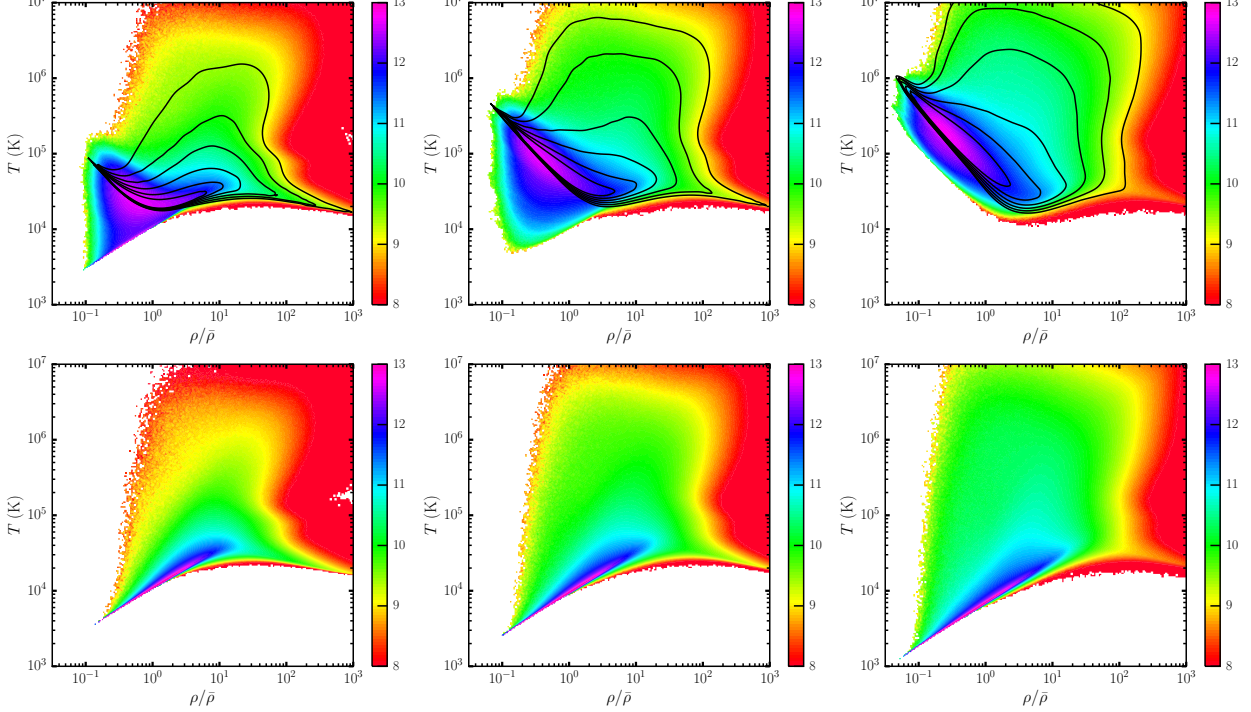


FIG. 2.— Volume-weighted temperature - density relation at  $z = 3, 2$  and  $1$  (from right to left) for the simulations with no blazar heating (bottom) and inhomogeneous heating (top). The overlying black contours show the corresponding  $T - \rho$  relation for uniform blazar heating (Puchwein et al. 2012) for the same redshift range. The color scale is logarithmic.

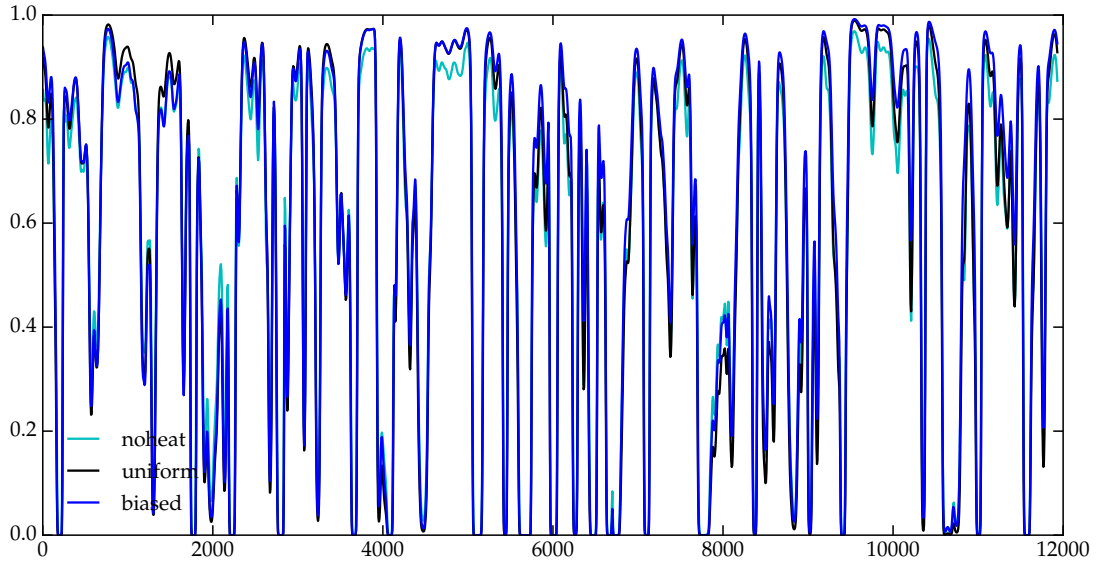


FIG. 3.— Ly $\alpha$  absorption spectrum at  $z = 2.2$  in the three models. [Placeholder, will be improved]

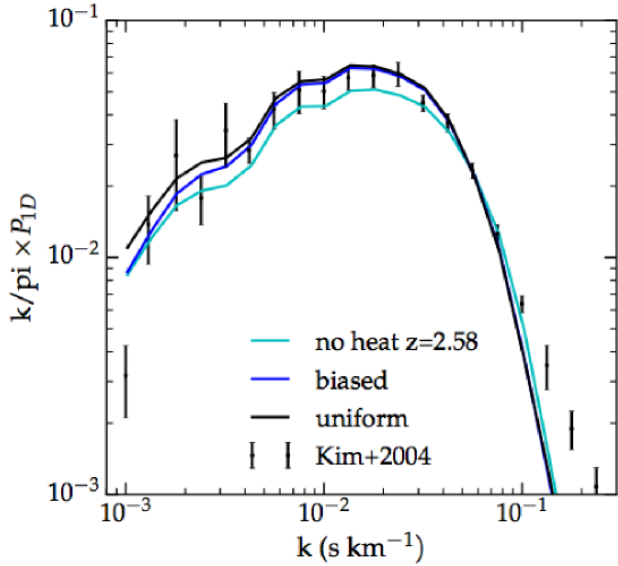


FIG. 4.— Power spectrum at different redshifts compare with observations [Placeholder, will be improved]

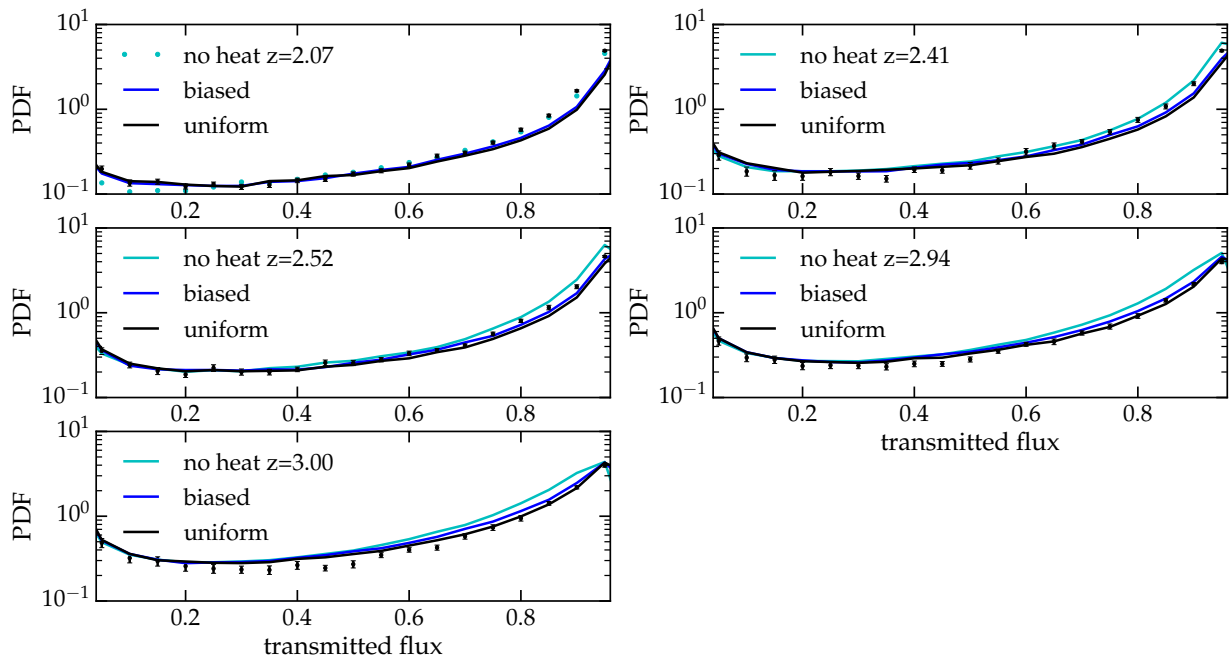


FIG. 5.— Flux PDF at different redshifts compare with observations [Placeholder, will be improved]

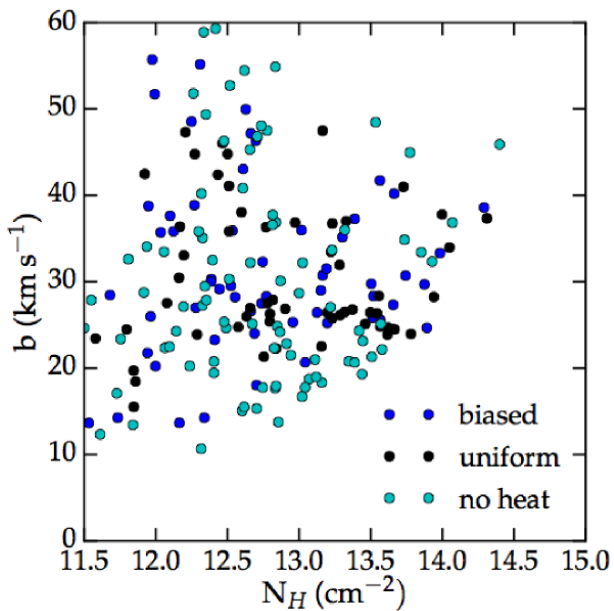


FIG. 6.— Column density - Doppler with distribution in the different models [Placeholder, will be improved]